Preprint Title	Evaluation of hemolytic activity and oxidative stress biomarkers in erythrocytes after exposure to bioactive glass nanoceramics
Authors	Ioannis Tsamesidis, Konstantina Kazeli, Georgia Pouroutzidou, Karine Reybier, Antonella Pantaleo, Evgenia Lymperaki and Eleana Kontonasaki
Publication Date	14 Aug 2019
Article Type	Full Research Paper
ORCID® iDs	Ioannis Tsamesidis - https://orcid.org/0000-0002-1439-3920

Title: Evaluation of hemolytic activity and oxidative stress biomarkers in erythrocytes after exposure to bioactive glass nanoceramics

Running Title: Hemolysis and oxidative stress of erythrocytes in contact with nanoceramics

Authors: Ioannis Tsamesidis[1,5a], Konstantina Kazeli[2,3], Georgia K. Pouroutzidou[4], Karine Reybier[5], Antonella Pantaleo[1], Evgenia Lymperaki[2], Eleana Kontonasaki[6]

Affiliations:

[1]Department of Biomedical Sciences, University of Sassari, Sassari 07100, Italy

[2] Department of Biomedical Sciences, National Hellenic University, Thessaloniki, Greece,

[3]Department of Medicine, Democritus University of Thrace, Alexandroupoli, Greece

[4]School of Physics, Faculty of Sciences, Aristotle University of Thessaloniki, 54124 Thessaloniki, Greece

[5] Pharmadev, UMR 152, Université de Toulouse, IRD, UPS, Toulouse, 31400, France.

[6]Department of Prosthodontics, School of Dentistry, Faculty of Health Sciences, Aristotle University of Thessaloniki, Thessaloniki, Greece, GR-54124

[a]Correspondence: Ioannis Tsamesidis, [1]Department of Biomedical Sciences, University of Sassari, Current affiliation: Pharmadev, UMR 152, Université de Toulouse, IRD, UPS, Toulouse, 31400, France. johntsame@gmail.com telephone number: +39 3926725338

Key words: bioactive glass-ceramic nanoparticles, red blood cells, hemolysis, ROS production

Abstract:

The nature of the surface is critical in determining the biological activity of silica powders. A novel correlation between toxicity and surface properties of bioactive glass ceramics (BGCs) synthesized via the sol-gel method was attempted in this study. The behavior of BGCs after their attachment to the surface of red blood cells (RBCs) was evaluated and their toxic effects were determined based on hemolysis, membrane injury via anti-phosphotyrosine immunoblot of Band 3, lipid peroxidation, potential to generate reactive oxygen species, and antioxidant enzyme production. In particular, three BGCs were synthesized at three calcination temperatures (T1=835 °C, T2=1000 °C and T3=1100 °C). Their toxicity based on hemolysis was dose dependent, while BGC-T2 had the best hemocompatibility in compare with the other BGCs. No BGCs in dosages lower than 0.125mg/ml could damage erythrocytes. On the other hand, all BGCs promoted the production of reactive oxygen species in certain concentrations, with the BGC-T2 producing the lowest ROS and increasing the glutathione levels in RBCs protecting their damage. The results suggest that various factors such as size, a probable different proportion of surface silanols, a balanced mechanism between calcium and magnesium cellular uptake or the different crystalline nature may have contributed to this finding; however, future research is needed to clarify the underlying mechanisms.

.

Introduction

Silica based ceramics have been the most widely used materials in medical practice, particularly in orthopedic applications[1–4]. These inorganic compounds have been selected due to their excellent cytocompatibility and *in vivo* biological responses. However, these bioceramics share a common disadvantage of being brittle, and as such cannot be used to replace tissues where extensive mechanical loading exists[5]. By structuring these bioceramics in the nanoscale, it is possible to overcome this limitation but is also necessary to evaluate their possible toxicity especially in erythrocytes[6–8]. Blood compatibility plays an important role for artificial implants and materials for tissue regeneration. When non-hemocompatible biomaterials come into contact with blood they could cause hemolysis through erythrocytes' membrane rupture[9]. One of the parameters affecting cell and protein attachment is the biomaterials' surface tension[10]. Surface tension in most cases depends on a multiplicity of factors associated with the types of individual or groups of atoms who are located on the surface[11]. It is well known that the structure of most of the biomaterials' surfaces is similar to that of a mosaic. The nature of the potential interaction sites and their topology determines the interactions of biomaterials with biological agents and particularly with blood[12]. One of the most serious problems that can be caused by the implant is hemolysis. In previous studies it has been demonstrated that the toxicity and hemolytic activity of silica nanoparticles depends on their size, geometry, porosity, and surface charge, due to the presence of silanol groups (OH-)[3,13]. It has been also reported that the reactivity of the silica surface and its ability to produce reactive oxygen species (ROS) may determine the hemolytic activity of these materials[14,15]. This ROS-based mechanism is likely to play a role in hemolysis caused by reactive surfaces.[16,17] Furthermore, nanoparticles mediated ROS generation can trigger the expression of pro-inflammatory cytokines and the recruitment of inflammatory cells, such as macrophages and neutrophils[18,19], it is also an effective option for the treatment of microbial induced infections[20]. Due to the high prevalence of antibiotic-resistant pathogens, strategies including ROS production from nanoparticles could contribute to the local control of infection in bone healing areas. For these reasons novel strategies should developed, based on a selective ROS generation towards microbial pathogens over the host tissue cells. The last few decades a lot of different compositions of ion-doped silica nanoparticles have been synthesized, as these materials can remarkably contribute to the multiple functions of biomedical materials in bone tissue engineering[21,22]. Their nanoscale nature presents a unique surface for the interaction with bone forming cells, thus promoting cell adhesion, proliferation and differentiation. Calcium phosphate (Ca-P) and calcium silicate (Ca-Si) nanomaterials can be applied as bone

filling materials, as coatings on bio-implant surfaces, as drug or molecule carriers, can be used to strengthen and induce bioactivity to various polymeric scaffolds and/or cements, while recently have been synthesized as magnetic nanoparticles for hyperthermia applications[23–26]. Calcium silicate bioceramics can induce ossification of various stem cell lines, such as bone marrow stromal cells [27–29], adipose derived stem cells, human dental pulp cells, and periodontal ligament cells[30]. In addition Ca-Si compositions containing compounds such as MgO have proven to develop apatite and stimulate osteoblasts-like cells (HOB) proliferation to a greater extent than β-TCP [31]. The aim of this study was the investigation of the toxic effects in erythrocytes after exposure to Bioactive glass ceramics (BGCs) and describe the sources and role of ROS in BGCs-related biological functions. The calcium silicate glass was synthesized by the Stöber method[32] in the ternary system SiO_2 55 –CaO 35 –MgO 10 mol% and heat treated at three different temperatures after thermogravimetric analysis (TGA/DTA) (BGC-T1 at 835 °C, BGC-T2 at 1000 °C, BGC-T3 at 1100 °C). The presence of free radical production by these particles could enable a clear distinction between the hemolytic activity resulting from morphologically different particles and from ROS generation.

Results:

A. Characterization of BGCs

Fourier transform infrared spectroscopy (*FTIR*) measurements

All three materials, irrespective of thermal treatment, exhibit the characteristic peaks of silicate glasses (as reported in the literature)[33–36]. In particular, the IR spectrum of silica glass consists of three main domains/areas: a) A strong wide peak at 1200-900 cm^{-1} with a centre of absorption at 1070 cm^{-1} and a shoulder at 1220 cm^{-1}, due to the asymmetric vibration of Si-O-Si. b) A strong peak at 580-400 cm^{-1} due to the asymmetric bending vibration of the O-Si-O bond. c) A peak at 800 cm^{-1}, due to the symmetric stretching vibration of the Si-O bond. In addition, in all spectra, a weak peak at 1640 cm^{-1} and a wide at 3470 cm^{-1} are observed and are attributed to the bending and stretching vibrations of the C-H bond, respectively, due to the presence of moisture in the sample. The weak peak at 3780 cm^{-1} attributes to the vibration of the O-H bond of the singular silanols Si-OH (alone silanols) groups. Finally, the very weak and broad peak at 1500-1400 cm^{-1} attributes to the asymmetric bond of C-O of the -CO$_3$ group due to the infiltration of CO$_2$ into the bioceramic. The spectra of the heat treated samples at 1000°C(BGC-T2) and 1100°C (BGC-T3) show new sharp peaks, indications of generation of crystalline phases in the material, as expected, compared to the sample which was heat treated at 835 °C (BGC-T1), which appears to be the most amorphous of all three. A distinct peak at 745 cm^{-1}, which is present only in the spectrum of BGC-T2, can probably be assigned to enstatite or clinoenstatite. [37–39]
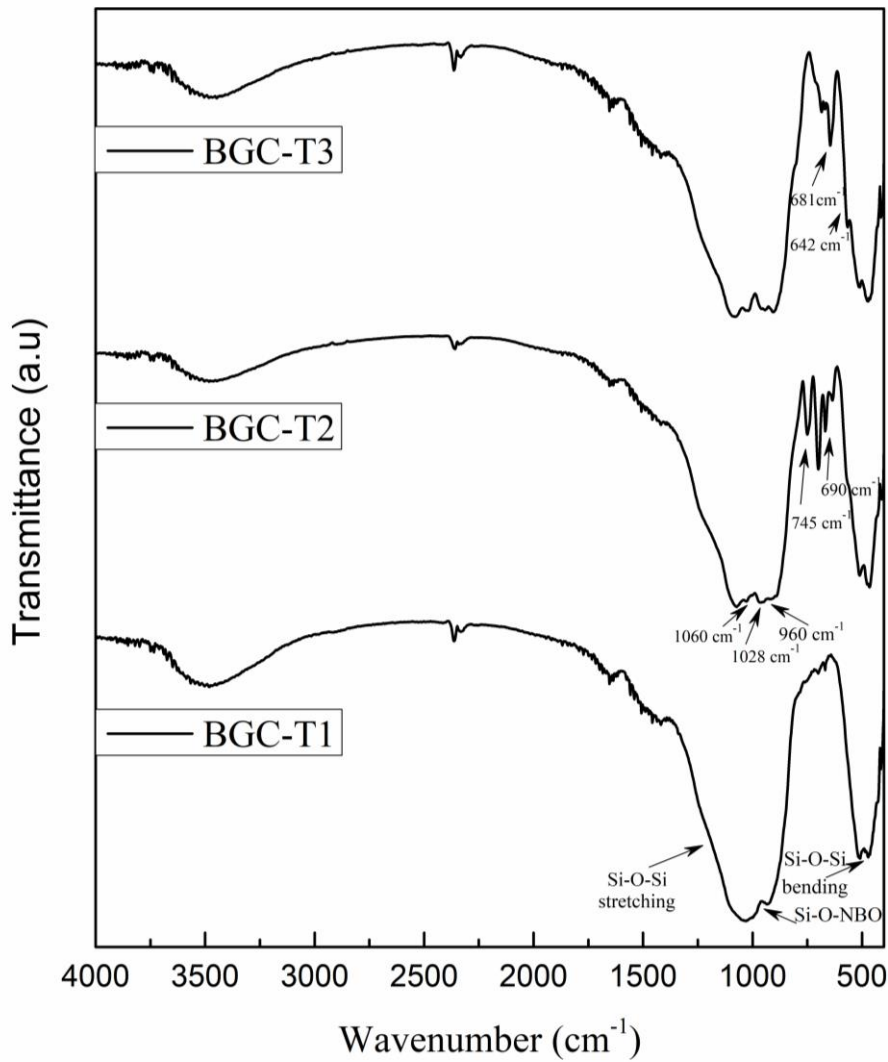
Figure 1. *FTIR spectra of produced bioactive glasses*

Particle size evaluation by laser dynamic light scattering (DLS) and surface area by gas adsorption (BET method)

The bioactive glass particle size and size distribution measured by DLS in physiological saline are shown in Fig. 2. As could be seen, the particles range from around 2.13 to 6.8 nm in physiological saline. The values were shown to be 2.13 nm ±0.43 for BGC-T1, 6.82 ±1.27 for BGC-T2, and 4.39 ± 0.8 for BGC-T3 (Table 2). The results showed that these particles are relatively agglomerated in physiological saline.
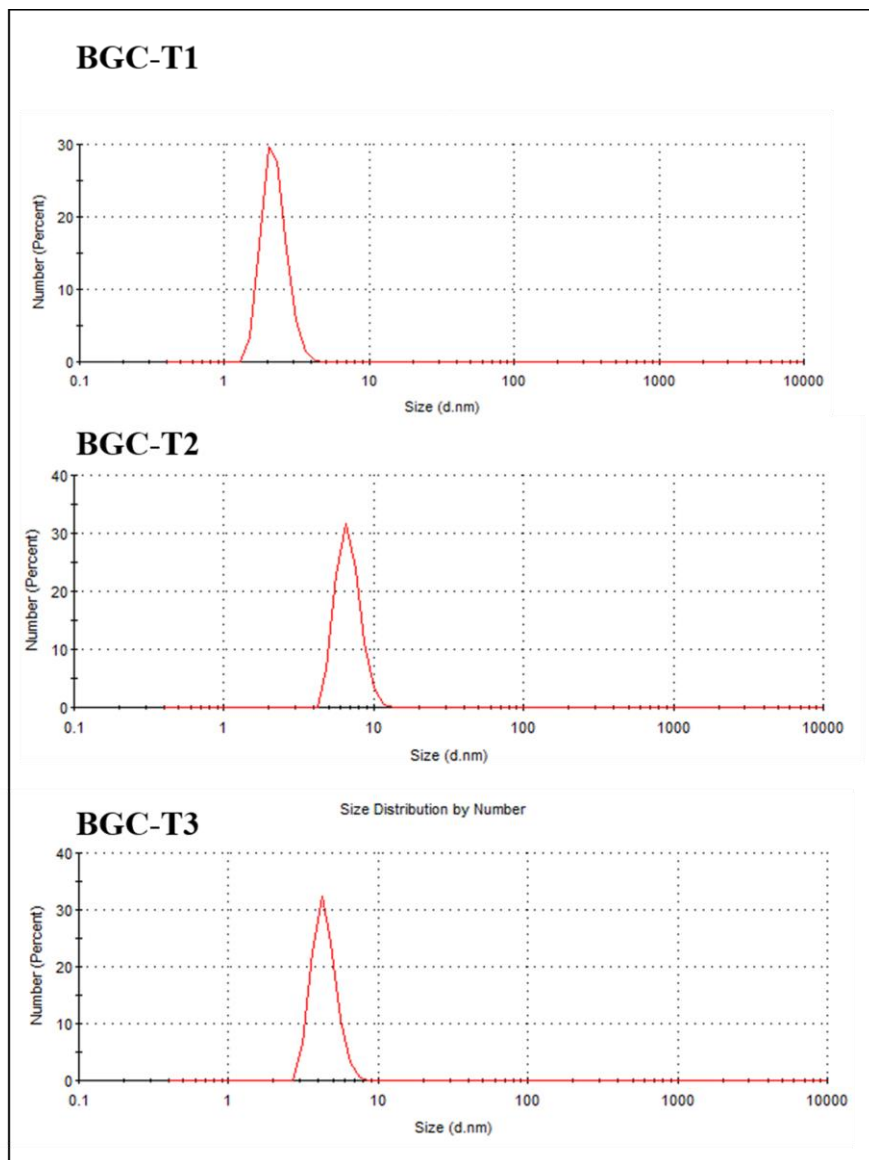
Figure 2. DLS analysis of synthesized ''bioactive glass ceramics''

Furthermore, the BET specific surface area of bioactive glass particles ranged from 22 to 48 m^2/g (Table 2).
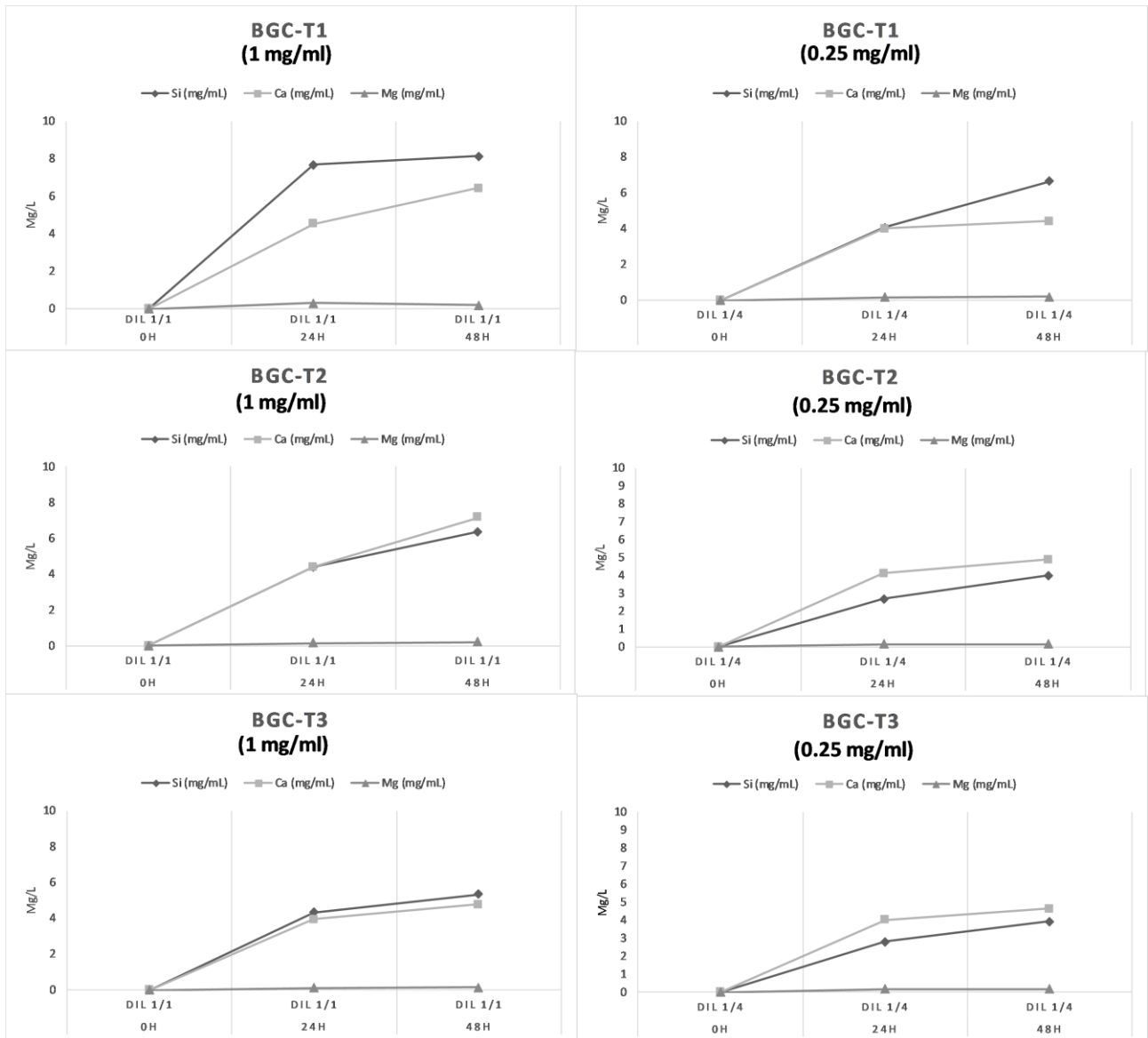
Table 2. Specific surface are and average size of BGCs

Bioactive nanomaterials	Specific Surface Area (m^2/g)	Average Size (nm)
BGC-T1	48	2.13±0.43
BGC-T2	29	6.82±1.27
BGC-T3	22	4.39± 0.8

Analysis of ions released from BGCs using inductively coupled plasma-atomic emission spectrometry – ICP/AES.

The ICP analysis was performed for each BGC sample, and Si^{4+}, Ca^{2+} and Mg^{2+} ions release was measured soon after the standard solutions of Si, Ca and Mg were prepared, followed by plotting the calibration (standard) curve. ICP results showed that both Si^{2+} and Ca^{2+} ions release in the analyzed solutions gradually increases during the first 24 hours of immersion and then a slightly smaller gradient linear increase is observed until the 48 h of incubation, whereas, Mg^{2+} ions remain in steady and lower values. Concerning the two concentrations (0.25 mg/mL, 1 mg/mL), a slight decrease is observed in the lower concentration. Higher values of ion release are present for BGC-T1 which is the most amorphous of all three samples. As the thermal treatment-annealing temperature increases, a slight decrease is detected to the ion release values of Si for both BGC-T2 and BGC-T3 and of Ca for BGC-T3.

Figure 3. A-F : *The variations of Si, Ca, and Mg ions release, measured by ICP method, for two different concentrations (0.25mg/ml right, 1mg/ml left) and two time points (24 h, 48 h) for all tested BGCs. The evaluated dilutions of the nanopowders (D) were 1/1 (left) and 1/4 (right). The values of Mg ion release were multiplied x10 in order its variations to be easily distinguished.*

B. Effect of RBC-BGCs interaction on RBC deformability

Hemolytic properties of BGCs

All silica based nanobioceramics induced dose-dependent hemolysis on red blood cell (RBC) after the first 24 hours of incubation damaging erythrocytes from 0.125 mg/mL till the highest tested concentration (Figure 4 A and B). The best hemocompatibility presented the composition of BGC-T2. The decreased hemolysis at BGC-T2 was attributed to the surface chemistry of silica, where the silica surface is populated by an equilibrium of silanol groups (SiOH) and ionized silanol groups (SiO_) upon contact with water. In order to assess the potential of BGCs in fragile erythrocytes we induced mechanical stress as previously described [40]. BGC-T2 and T3 presented protective effect under conditions of stress. Mechanical stress in BGC-treated erythrocytes promoted an improvement in the hemolytic activity in all the tested BGCs. With lower concentrations (0.03 to 0.5 mg/ml) of BGC-T2 and T3, the effect of mechanical stress on the hemolysis rates markedly decreased (Figure 4C), suggesting a directly toxic effect of higher concentrations of BGCs in erythrocytes.
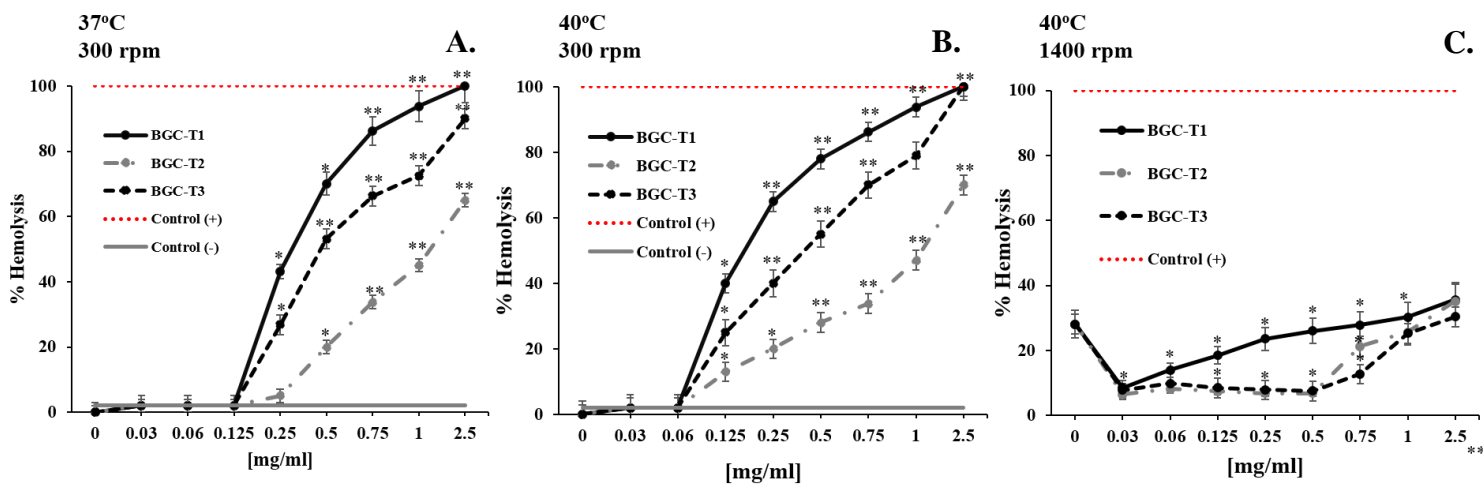

Figure 4. *Hemolytic action of BGs in PBS with normal erythrocytes under different conditions of treatment (different temperatures (37 and 40 ^{O}C) and* shaking*. The results are expressed as % of positive control (hemolysis buffer). Data are mean ± SEM (n=6 in each group).* ✱ *Significant differences to control (-) at p < .05 ✱✱ p < .001*

Confocal microscopy analysis and anti-phosphotyrosine immunoblot of Band 3

Figure 5 illustrates the confocal microscopy analysis in control (A) and BGC-T2 (B, C and D) treated erythrocytes at different concentrations (0.125, 0.5 and 1mg/mL respectively). The erythrocytes in the control group displayed a typical concave disk and relatively uniform shape and size. BGC-T2-treated erythrocytes appeared a dose dependent behavior performing swollen, erythrocyte membrane modification, and even membrane fragments. RBCs deformability increased in a dose-dependent manner causing eryptosis at high concentrations highly associated with erythrocyte injuries.
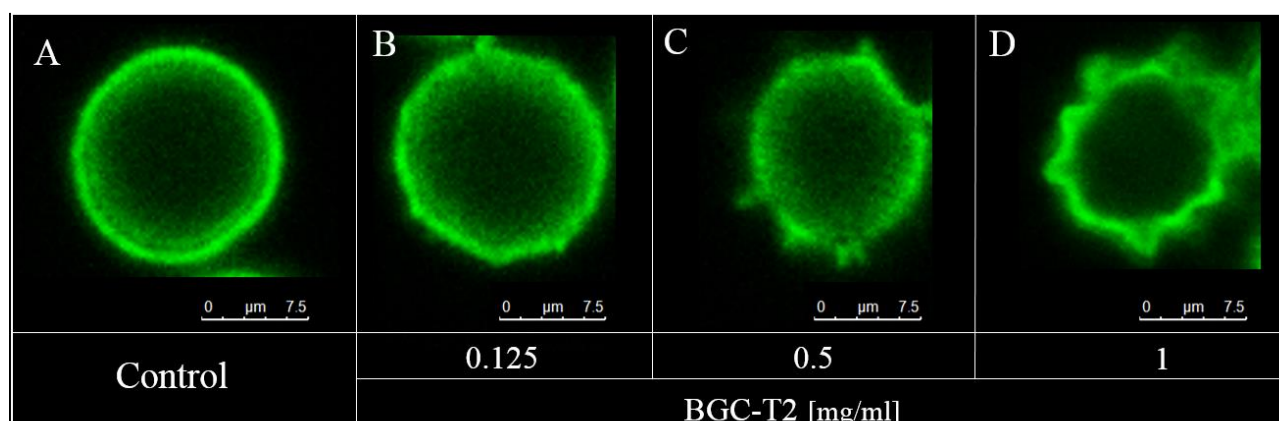

Figure 5. *Confocal images of erythrocytes after treatment with different concentrations (0.125, 0.5 and 1 mg/ml) of BGC-T2 (scale bar 10 μm)*

Once we demonstrated the erythrocyte membrane modifications, we then compared tyrosine phosphorylation of Band 3 in BGC-T2 treated erythrocytes with untreated erythrocytes. As shown in Figure 6, phosphorylation of Band 3 in untreated erythrocytes is almost undetectable, whereas its phosphorylation in BGC-T2 treated erythrocytes is prominent.
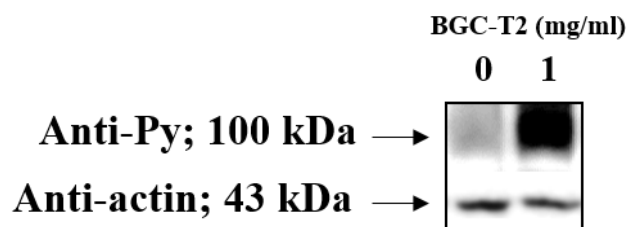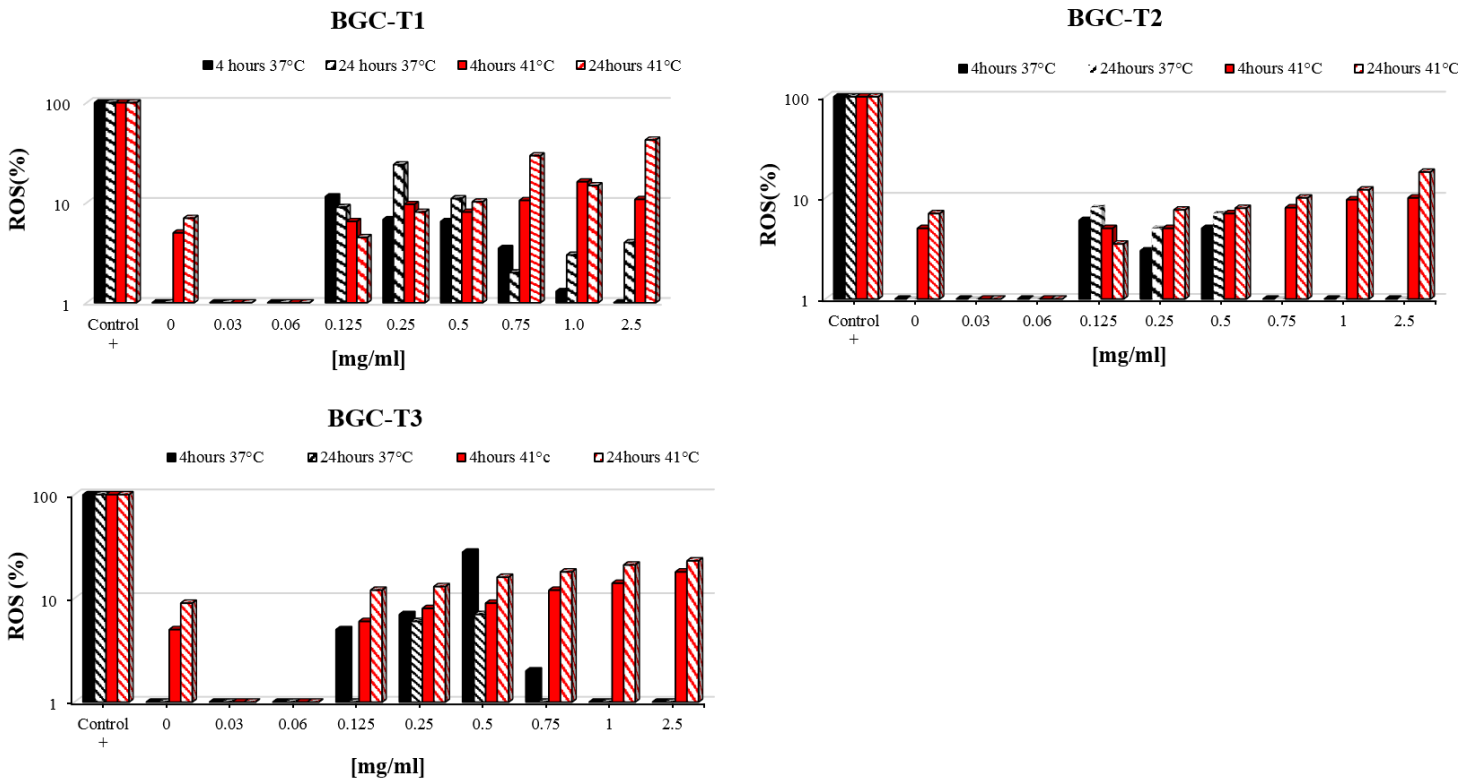

Figure 6. *Representative anti-phosphotyrosine immunoblot of Band 3 in erythrocyte membranes from BGC-T2-treated healthy volunteer erythrocytes*

C. Evaluation of oxidative stress biomarkers in BGCs treated erythrocytes

Production of ROS

Figure 7 shows that all BGCs induced increase of ROS generation after the first 4 hours of incubation in concentrations from 0.125mg/ml to 0.5mg/ml. BGC-T2 presented the lower total amount of ROS in erythrocytes and in groups 0.75, 1 and 2.5 significantly decreased the amount of ROS in compare with the other BGCs ($p < 0.05$). With increasing the temperature of incubation the reactive oxygen species (ROS) activity of RBCs increased accordingly. Time course studies of bioactive glass ceramics at different concentrations were performed, and no significant increase or decrease of ROS levels was observed at any time point or at any concentration when compared with the controls.

Figure 7. *ROS production in erythrocytes treated with all the tested BGCs*

Reduced glutathione (GSH) and lipid peroxidation analysis

BGC-T2 after 24 hours of incubation showed an increase of GSH levels by 33%, 40%, 52% and 55% in erythrocytes exposed to 0.125, 0.25, 0.5, 0.75 mg/mL, respectively, when compared to controls (Figure 8). There was a marginal reduction of GSH levels in erythrocytes treated with BGC-T1 and BGC-T3 and a consequent tendency in lipid peroxidation. In contrast to low GSH activity, BGC- T1 promoted a significant increase of lipid peroxidation at all the tested concentrations, except intermediate concentrations of 0.5 and 0.75 mg/mL. A statistical significant inverse correlation between GSH and MDA levels has been observed in all BGCs-treated erythrocytes. Our results indicate that BGC-T2 exposure in RBC can promote ROS production without disturbing GSH levels and avoiding lipid peroxidation in concentrations lower than 0.75 mg/ml.
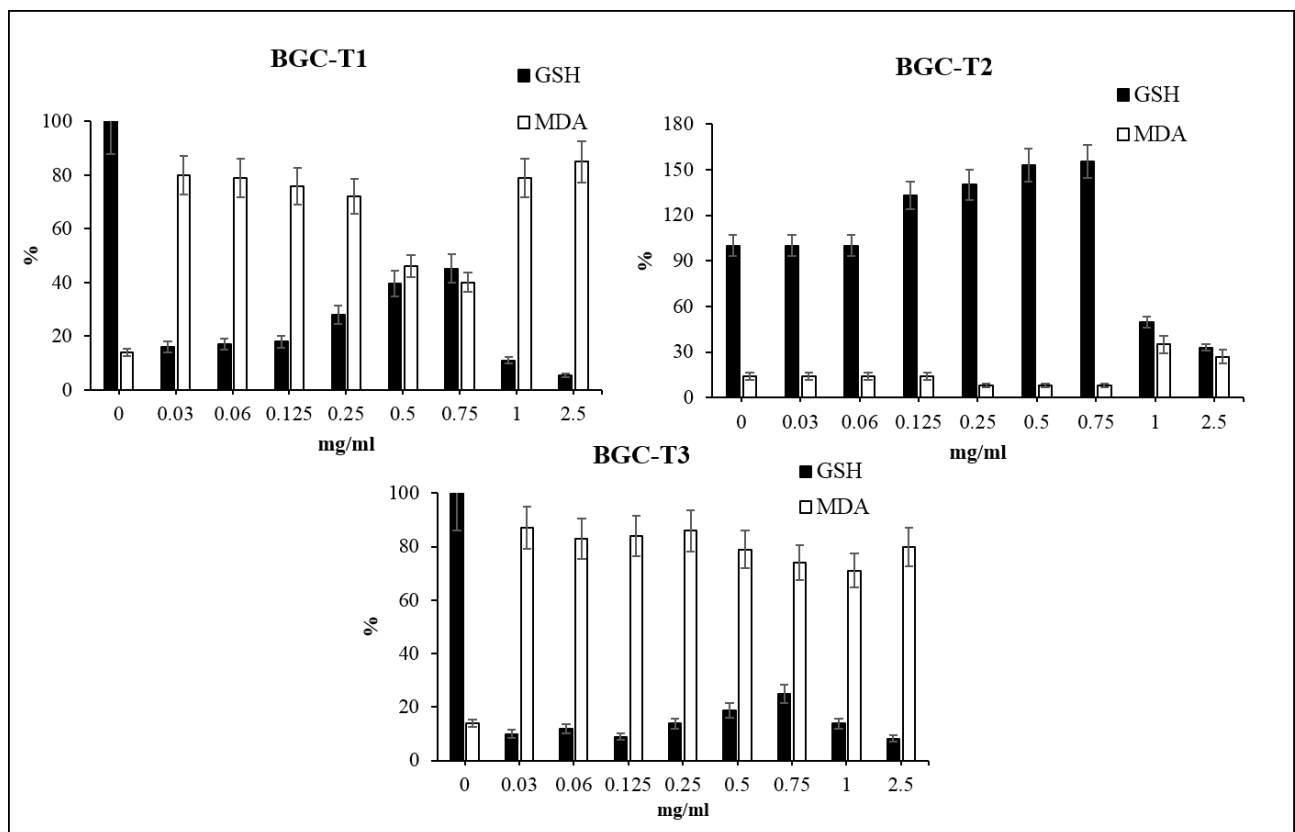

Figure 8. *GSH and MDA levels in erythrocytes treated with all the tested BGCs*

Material and Methods:

13

Unless otherwise stated, all materials were obtained from Sigma-Aldrich, St. Louis, MO, USA.

Synthesis of bioactive glass ceramics

In the present study, nanosized bioceramics in the system $SiO_2CaOMgO$ (55, 35 and 10%mol respectively) were synthesized by the Stöber-based sol-gel method. Silicon oxide was added in the form of a TEOS solution while Mg and Ca were added as nitrate salts in a mixture of d.d H_2O, ethanol (ethanol:teos=10:1) and HNO_3, after the hydrolysis of TEOS. Following, ammonia solution (10 ml) was inserted dropwise under stirring in ultrasonic bath. The initial bioceramic was thermally treated from 30 °C to 1380 °C with a rate of 10 °C / min in air conditions. Based on the results of thermal analysis, the initial material was divided into three isomeric quantities and was heated to three different temperatures for further study (835 ° C, 1000 ° C, 1100 ° C)[41–43].

Table 1: Composition of all synthesized bioactive glass ceramics

Bioactive glass ceramics		
Bioactive nanomaterials	Composition(mol)	Calcination Temperature (C°)
BGC-T1	55-35-10% $SiO_2CaOMgO$	835
BGC-T2	-//-	1000
BGC-T3	-//-	1100

Fourier Transform Infrared Spectroscopy (FTIR)

The synthesized materials were characterized by Fourier Transform Infrared Spectroscopy (FTIR). The bioceramic glass powder samples were analyzed at room temperature in the wavenumber range of 4000-400cm^{-1}(MIR) with a Fourier transform infrared spectrometer (Spectrum 1000, PerkinElmer), with a resolution of 4cm^{-1} and 32scans.

Brunauer-Emmett-Teller (BET)

The specific surface area (SSA) values of the composite nanopowders are shown in Table 2. The specific surface area of the materials was estimated by nitrogen gas adsorption at liquid phase temperature (77 K) using a micropore surface analyzer according to the Brunauer-Emmett-Teller (BET) model.

Inductively coupled plasma-atomic emission spectrometry (ICP-AES)

The three thermally treated bioceramic nanopowders (BGC-T1, BGC-T2 and BGC-T3) were individually immersed and diluted in 5 mL solution of DI water and PBS (95% DI water, 5% PBS) for two different BGC concentrations (0.25 mg/mL, 1mg/mL)- based on the upper and lower dose dependence limit for haemolysis assay- and incubated for 24 h and 48 h. The ICP analysis was performed for each BGC sample solution, and Si^{4+}, Ca^{2+} and Mg^{2+} ions release was measured soon after the standard solutions of Si, Ca and Mg were prepared, using the external standards calibration curve. For the analysis by ICP, a Perkin Elmer (USA) model OPTIMA 3100 XL AxialViewing Spectrometer was used. The spray chamber is Scott's dual-pass mode. The nebulizer uses a GemTip cross-flow pneumatic type and allows analysis of solutions containing dissolved solids up to 5%. The power source includes a free-running 40 MHz radio frequency generator, and the plasma gas is high purity in argon (99.995%). The optical system consists of echelle grating and a solid phase detector belonging to the category of Charged Coupled Detectors. Specific wavelengths were used for each element analyzed: Si=251.611 nm, Ca=396.847 nm and Mg=280.271 nm.

Dynamic Light scattering (DLS)

The particle size distribution of the BGCs in water dispersion was determined by dynamic light scattering using a particle size analyzer (Zetasizer nano ZS, Malvern Instruments Ltd., U.K.) at 25 °C with 90° detection angle.

Ethics Statement

Venous blood was drawn from six healthy individuals. All subjects provided written, informed consent before entering the study. The study was approved by the local Ethics Committee and conducted in accordance with Good Clinical Practice guidelines and the Declaration of Helsinki.

Hemolysis assay

RBCs were separated from plasma and leukocytes by washing three times with PBS. To determine the haemolytic activity on Red blood cells (RBCs), BGCs suspension (stock = 5 mg/ml) prepared with sterile isotonic PBS 1X was added to diluted RBCs at different concentrations (0.03, 0.06, 0.125, 0.25, 0.5, 0.75, 1, 2.5 mg/ml) for 24 and 48 hours of incubation at 37 ˚C and 41 ˚C (Thermomixer-Biosan). PBS 1X was used as a negative control (Ctrl-) and hemolysis buffer (5 mmol/L sodium phosphate, 1 mmol/L EDTA, pH 8.0) was used as positive control (Ctrl +). Then, samples were centrifuged at 2000 rpm for 1 minute and a microplate reader (Thermo Scientific) was used to measure the absorbance of haemoglobin release in the supernatant. The absorbance value of haemoglobin at 541 nm was measured with the reference wavelength of 700 nm. The percent of hemolysis was calculated as follows: Hemolysis % = [(sample absorbance -negative control) / (positive control - negative control)] * 100%.

Quantitation of Band 3 Tyrosine Phosphorylation

Washed RBCs were suspended at 30% hematocrit in PBS-Glucose and treated with the most hemocompatible BGC, BGC-T2 (1 mg/ml) for 24 hours at 37°C under 50 rpm shaking. RBC ghosts were then prepared by mixing 50 µL of packed RBCs with 1500 µL of ice-cold ghost buffer (5 mM Na_2HPO_4, 1 mM EDTA, pH 8.0, containing 1 mM phenylmethylsulfonyl fluoride (PMSF) and 1% phosphatase cocktail inhibitors 2 and 3, and allowed to sit on ice for 30 min. Samples were centrifuged at 13000 rpm for 15 min at 4 °C and supernatants were removed. Band 3-tyrosine phosphorylation was quantitated by loading 30 µL of each thawed sample onto an 8% SDS-PAGE gel. Proteins were then transferred to a nitrocellulose membrane at 100 V, after which membranes were immunostained with anti-phosphotyrosine (1:1000, Cell Signaling Inc.) or anti-actin (1:20000) antibodies. Quantitative densitometry analysis was performed using Odyssey V3.0 software.

Mechanical fragility assay

Mechanical fragility assay was performed on freshly obtained erythrocytes in the presence of an anticoagulant. All erythrocytes samples were subjected simultaneously to the same mechanical stress. RBC and RBC-BGCs suspensions were mixed vigorously for 24 hours at 40 °C at 1400 rpm. The hemoglobin released from the RBCs during mixing was immediately assayed as previously described in hemolysis assay section.

Preparation of red cells treated with BGCs for confocal microscopy

RBCs treated for 24 hours with BGC-T2 were pelleted and washed twice in PBS containing 5 mM glucose and then fixed for 5 min in 0.5% acrolein in PBS. Cells were rinsed three times, then permeabilized in PBS containing 0.1 M glycine (rinsing buffer) plus 0.1% Triton X-100 for 5 min, and rinsed again 3× in rinsing buffer. To ensure complete neutralization of unreacted aldehydes, the cells were then incubated in rinsing buffer at room temperature for 30 min. After incubation, all nonspecific binding was blocked by incubation for 60 min in blocking buffer (PBS containing 0.05 mM glycine, 0.2% fish skin gelatin and 0.05% sodium azide). Resuspended RBCs were allowed to adhere to polylysine-coated cover slips, after which the cover slips were mounted with Aqua-Mount (Lerner Laboratories, New Haven, CT).

Fluorescence analysis for the detection of ROS levels

For the detection of intracellular reactive oxygen species (ROS) levels, we employed the cell-permeable ROS-sensitive probe 2',7'-dichlorodihydrofluorescein diacetate (CM-H$_2$DCFDA) which fluoresces at 520 nm (λex=480 nm) upon oxidation. Oxidation of CM-H$_2$DCFDA (prepared as a 0.5 mM stock solution in DMSO) in RBCs was monitored by measurement of the fluorescence of the desired RBC suspensions (0.2% Hematocrit) in 96-well black-walled microplates (Corning®, Sigma Aldrich) using a SAFAS Xenius (Monaco). The relative fluorescence is expressed as "% maximal emission" as determined with the software ''Xenius'', where maximal emission was defined as the fluorescence emission obtained following addition of 3 mM H$_2$O$_2$.

Reduced Glutathione (GSH) evaluation

Reduced Glutathione (GSH) was measured colorimetrically after 24 hours exposure in different concentrations of BGCs, using a glutathione assay Kit by Cayman Chemical Company utilizing enzymatic recycling method. GSH levels were compared with the control values.

Malondialdehyde (MDA) evaluation

Lipid peroxidation status in erythrocytes treated with BGCs was determined by estimating colorimetrically malondialdehyde (MDA) as thiobarbituric acid reactive substances at 532nm, prior to dialysis using a TBARS assay kit by Cayman Chemical Company (Ann Arbor, MI). MDA levels were compared with the control values.

Discussion:

To be clinically applicable, bioactive glass ceramics (BGCs) must not induce severe adverse effects on red blood cells (RBCs). The haemolytic activity of BGC-T1, BGC-T2 and BGC-T3 was evaluated in order to identify which thermal treatment possess the best hemocompatibility and could be efficiently applied in bone tissue engineering. The hemolysis assay is commonly performed at body and fever temperature (37 °C and 41 °C) at concentrations ranging from 0.03 to 2.5 mg/mL till 24 hours of incubation and thus this protocol was applied in the present study. All silica based nanoparticles induced dose-dependent hemolysis on red blood cell (RBC) after the first 24 hours of incubation damaging erythrocytes from 0.125 mg/mL till the highest tested concentration. At fever temperature hemolysis of all BGCs was appeared at 0.06 mg/ml and increased 15-30% in compare with the physiological conditions in line with previous findings [44]. The hemolytic effects on RBCs is strongly related to factors such as nanoparticle porosity, geometry, and surface functionality[13]. It is well-known that external surface area affects hemolysis, by either modulating the number of RBCs that bind to nanoparticles or by affecting the energy of cell membranes to wrap around nanoparticles[45]. In the present study, specific surface area as measured by BET showed values ranging from 22 to 48m^2/g, which is common to silica nanoparticles prepared by the Stöber method[13]. As high surface area renders hemolysis thermodynamically favorable, it can be suggested that the highest hemolytic activity of BGC-T1 is justified by its highest surface area. On the contrary, the lowest hemolytic activity of BGC-T2 cannot be solely explained by its low surface area, as it differs only slightly compared to that of BGC-T3 which presented higher hemolytic activity. Different ratios of Si–OH (silanols) to Si–O–Si (siloxane bridges) groups on the surfaces of the materials have been recorded under various thermal treatments. In general, heating and annealing at temperatures up to 800°C decrease the amount of silanols present at the surface, by their progressive condensation into stable unreactive siloxane bridges. Physically bound water and hydrogen-bonded silanols are removed first (Figure 1), creating closed siloxane rings and progressively increasing surface hydrophobicity. Although distinct differences in the amounts of silanols could not be verified by FTIR, it is expected that the BGC-T1 has a higher number of external surface silanols compared to both ceramics heat treated at elevated temperatures[46] and that the decreased hemolysis with BGC-T2 could be attributed to a different equilibrium of silanol (SiOH) and ionized silanol groups (SiO_) upon contact with water. However, nanoparticle interactions at the nano/bio interface are governed by a variety of properties such as chemical composition, surface functionalization, shape, angle of curvature, porosity, crystallinity, heterogeneity, roughness, and hydrophobicity or hydrophilicity[6]. Apart

from the concentration of surface silanols, the relative proportion of strained and unstrained siloxane rings on the surface of silica nanoparticles has been suggested to affect hemolysis[21]. Although Stöber silica synthesis involves principally unstrained four-membered and larger rings, thermally promoted condensation reactions can result in the formation of strained surface-associated 3MRs. In aqueous environment, the siloxane bonds of the strained three-membered rings (3MRs) are distorted and reactive oxygen species (ROS) are formed, which may result in hemolysis. The lowest hemolytic activity of BGC-T2 was accompanied by the lowest ROS production, suggesting a lower number of distorted strained siloxanes. Another factor crucial for activating hemolysis is the intracellular Ca^{2+}, as it triggers several downstream events in RBCs[47]. Increased Ca^{2+} levels lead to the disruption of the asymmetrical distribution of phospholipids in the plasma membrane and erythrocyte death could be triggered by increased intracellular calcium[48,49], entered through non-selective cation channels activated by oxidative stres[50]. In erythrocytes, intracellular Ca^{2+} levels are monitored by the balance between calcium influx through the plasma membrane and calcium efflux regulated by the ATP-dependent Ca pump[51,52]. In particular, the intracellular calcium concentration is regulated by a particulate calmodulin-dependent Ca^{2+} Mg^{2+}-ATPase and the disturbance of its activity can damage erythrocytes causing hemolysis[49]. The release of calcium presented slight differentiations among the studied nanoparticles that cannot be used to dictate possible differences in cellular uptake that could eventually tailor the hemolytic activity. On the other hand, BGC-T2 nanoparticles contain high amounts of enstatite ($Mg_2Si_2O_6$), which has been correlated to low hemolytic potential in rat RBCs[39]. Furthermore, oxidative stress leads to inactivation of erythrocyte tyrosine phosphatases[53] that in turn allows tyrosine phosphorylation of Band 3 by constitutively active tyrosine kinases to proceed unimpeded [54]. Tyrosine phosphorylation induces an intramolecular interaction in Band 3 in RBCs treated with high concentration of BGCs that causes dissociation of the spectrin/actin cortical cytoskeleton from the membrane[55] and the consequent destabilization and fragmentation of the membrane. These data demonstrate that BGC-T2 in high concentrations interact with the red blood cell membrane tyrosine kinases that naturally phosphorylate Band 3.

It seems possible that various combining factors such as the slightly higher size, a probable different proportion of surface silanols, a balanced mechanism between calcium and magnesium cellular uptake or the different crystalline nature, may have contributed to the lower hemolytic activity and less oxidative stress induced by the BGC-T2 nanoparticles. Moreover, the nature of the protein corona affected by the above parameters and controlled by the available nanoparticles' surface ligands, may further modify the erythrocytes responses[56]. Further studies are needed to

elucidate the underlying mechanisms. A dose dependent increase in the hemolytic properties of the BGCs was recorded, which is in accordance to many other studies. This behavior is accompanied to a clear RBCs membrane distortion as evidenced by confocal microscopy (Figure 5), leading finally to rupture at high concentrations. As the thermal treatment-annealing temperature increases, a slight decrease is detected to the ion release values of Si and Ca, attributed to the more stable network that the (more) crystalline phases forms that resists degradation. Regarding the ions release in relation to hemolytic (1mg/ml) and non-hemolytic (0.25mg/ml) concentrations, substantial differences were not observed, providing further evidence that a combination of various balancing mechanisms are responsible for the different behavior in relation to hemolysis.

Conclusions

In this study, new insights on the interaction between different heat-treated bioactive glass nanoceramics and the RBC membrane have been provided. All synthesized materials presented non-hemolytic activity at low concentrations, while only after thermal treatment at intermediate temperature a balance between ROS generation and antioxidative behavior was achieved. Various factors may have contributed to this finding; however, future research is needed to clarify the underlying mechanisms.

References

1 Progress S & Approaches N *Clinical Applications of Biomaterials. NIH Consens Statement Online*.

2 Hench LL (1991) Bioceramics: From Concept to Clinic. *J. Am. Ceram. Soc.* **74**, 1487–1510.

3 Prabhu M, Kavitha K, Manivasakan P, Rajendran V & Kulandaivelu P (2013) Synthesis, characterization and biological response of magnesium- substituted nanobioactive glass particles for biomedical applications. *Ceram. Int.* **39**, 1683–1694.

4 Yan J, Estévez MC, Smith JE, Wang K, He X, Wang L & Tan W (2007) Dye-doped nanoparticles for bioanalysis. *Nano Today* **2**, 44–50.

5 Gupta R & Kumar A (2008) Bioactive materials for biomedical applications using sol-gel technology. *Biomed. Mater.* **3**.

6 Andre N, Tian X, Lutz M & Ning Li (2006) Toxic Potential of Materials at the Nanolevel. *Science (80-.).* **311**, 622–627.

7 Maynard AD, Aitken RJ, Butz T, Colvin V, Donaldson K, Oberdörster G, Philbert MA, Ryan J, Seaton A, Stone V, Tinkle SS, Tran L, Walker NJ & Warheit DB (2006) Safe handling of nanotechnology. *Nature* **444**, 267–269.

8 Oberdoester G (2010) Nanotoxicology: An Emerging Discipline Evolving from Studies of Ultrafine Particles (vol 113, pg 823, 2005). *Environ. Health Perspect.* **118**, A380–A380.

9 Banerjee R, Nageswari K & Puniyani RR (1997) Hematological aspects of biocompatibility - Review article. *J. Biomater. Appl.*

10 Wang HJ, Cao Y, Sun YY, Wang K, Cao C, Yang L, Zhang YD, Zheng Z, Li D, Wang JY & Han YL (2011) Is there an optimal topographical surface in nanoscale affecting protein adsorption and cell behaviors? *J. Nanoparticle Res.*

11 Balani K, Verma V, Agarwal A & Narayan R (2015) *Biosurfaces: A Materials Science and Engineering Perspective*.

12 Barrère F, Mahmood TA, de Groot K & van Blitterswijk CA (2008) Advanced biomaterials for skeletal tissue regeneration: Instructive and smart functions. *Mater. Sci. Eng. R Reports*.

13 Yu T, Malugin A & Ghandehari H (2011) Impact of Silica Nanoparticle Design on Cellular Toxicity and Hemolytic Activity. , 5717–5728.

14 Cash TP, Pan Y & Simon MC (2007) Reactive oxygen species and cellular oxygen sensing. *Free Radic. Biol. Med.* **43**, 1219–1225.

15 Chang JS, Chang KLB, Hwang DF & Kong ZL (2007) In vitro cytotoxicitiy of silica nanoparticles at high concentrations strongly depends on the metabolic activity type of the cell line. *Environ. Sci. Technol.* **41**, 2064–2068.

16 Wang F, Gao F, Lan M, Yuan H, Huang Y & Liu J (2009) Oxidative stress contributes to silica nanoparticle-induced cytotoxicity in human embryonic kidney cells. *Toxicol. Vitr.* **23**, 808–815.

17 Park EJ & Park K (2009) Oxidative stress and pro-inflammatory responses induced by silica nanoparticles in vivo and in vitro. *Toxicol. Lett.* **184**, 18–25.

18 Dayem AA, Hossain MK, Lee S Bin, Kim K, Saha SK, Yang GM, Choi HY & Cho SG (2017) The role of reactive oxygen species (ROS) in the biological activities of metallic nanoparticles. *Int. J. Mol. Sci.* **18**.

19 Manke A, Wang L & Rojanasakul Y (2013) Mechanisms of nanoparticle-induced oxidative stress and toxicity. *Biomed Res. Int.* **2013**.

20 Dryden M (2017) Reactive oxygen therapy: A novel therapy in soft tissue infection. *Curr. Opin. Infect. Dis.* **30**, 143–149.

21 Paul W & Sharma CP (2009) Nanoceramic Matrices: Biomedical Applications. *Am. J. Biochem. Biotechnol.* **2**, 41–48.

22 Feng J & Thian ES (2013) Applications of nanobioceramics to healthcare technology. *Nanotechnol. Rev.* **2**, 679–697.

23 Degli Esposti L, Carella F, Adamiano A, Tampieri A & Iafisco M (2018) Calcium phosphate-based nanosystems for advanced targeted nanomedicine. *Drug Dev. Ind. Pharm.* **44**, 1223–1238.

24 Khandan A & Ozada N (2017) Bredigite-Magnetite (Ca7MgSi4O16-Fe3O4) nanoparticles: A study on their magnetic properties. *J. Alloys Compd.* **726**, 729–736.

25 Liu X, Li M, Zhu Y, Yeung KWK, Chu PK & Wu S (2016) The modulation of stem cell behaviors by functionalized nanoceramic coatings on Ti-based implants. *Bioact. Mater.* **1**, 65–76.

26 Liverani L, Lacina J, Roether JA, Boccardi E, Killian MS, Schmuki P, Schubert DW & Boccaccini AR (2018) Incorporation of bioactive glass nanoparticles in electrospun PCL/chitosan fibers by using benign solvents. *Bioact. Mater.* **3**, 55–63.

27 Liu Q, Cen L, Yin S, Chen L, Liu G, Chang J & Cui L (2008) A comparative study of proliferation and osteogenic differentiation of adipose-derived stem cells on akermanite and β-TCP ceramics. *Biomaterials* **29**, 4792–4799.

28 Theocharidou A, Bakopoulou A, Kontonasaki E, Papachristou E, Hadjichristou C, Bousnaki M, Theodorou G, Papadopoulou L, Kantiranis N, Paraskevopoulos K & Koidis P (2017) Odontogenic differentiation and biomineralization potential of dental pulp stem cells inside Mg-based bioceramic scaffolds under low-level laser treatment. *Lasers Med. Sci.* **32**, 201–210.

29 Li H, Xue K, Kong N, Liu K & Chang J (2014) Silicate bioceramics enhanced vascularization and osteogenesis through stimulating interactions between endothelia cells and bone marrow stromal cells. *Biomaterials* **35**, 3803–3818.

30 Zhang X, Han P, Jaiprakash A, Wu C & Xiao Y (2014) A stimulatory effect of Ca3ZrSi2O9 bioceramics on cementogenic/osteogenic differentiation of periodontal ligament cells. *J. Mater. Chem. B* **2**, 1415–1423.

31 Mohammadi H, Hafezi M, Nezafati N, Heasarki S, Nadernezhad A, Ghazanfari SMH & Sepantafar M (2014) Bioinorganics in Bioactive Calcium Silicate Ceramics for Bone Tissue Repair : Bioactivity and Biological Properties. **12**, 1–12.

32 Hench LL & West JK (1990) The Sol-Gel Process. *Chem. Rev.* **90**, 33–72.

33 Griffiths PR (1983) Fourier transform infrared spectrometry. *Science (80-.).* **222**, 297–302.

34 Brückner R (1970) Properties and structure of vitreous silica. I. *J. Non. Cryst. Solids* **5**, 123–175.

35 Serra J, González P, Liste S, Serra C, Chiussi S, León B, Pérez-Amor M, Ylänen HO & Hupa M (2003) FTIR and XPS studies of bioactive silica based glasses. *J. Non. Cryst. Solids* **332**, 20–27.

36 (Ed) FV (1974) *Farmer VC (1974) 'The Anhydrous Oxide Minerals', In: Farmer VC (Ed), Infrared spectra of minerals in Mineralogical, Society Monograph 4, London: Mineralogical Society, pp. 183-204.*

37 Kalinkina E V., Kalinkin AM, Forsling W & Makarov VN (2001) Sorption of atmospheric carbon dioxide and structural changes of Ca and Mg silicate minerals during grinding I. Diopside. *Int. J. Miner. Process.* **61**, 273–288.

38 Kalinkina E V., Kalinkin AM, Forsling W & Makarov VN (2001) Sorption of atmospheric carbon dioxide and structural changeof Ca and Mg silicate minerals during grinding II. Enstatite, åkermanite and wollastonite. *Int. J. Miner. Process.* **61**, 289–299.

39 KOSHI K, HAYASHI H & SAKABE H (2009) Biological and Mineralogical Studies on Serpentine Minerals in Heat Treated State. *Ind. Health* **7**, 66–85.

40 Red blood cells under mechanical stress (1990) *Gen. Physiol. Biophys.* **9**, 291–299.

41 Wu C & Chang J (2004) Synthesis and apatite-formation ability of akermanite. *Mater. Lett.* **58**, 2415–2417.

42 C. W, J. C, W. Z, S. N & J. W (2006) Porous akermanite scaffolds for bone tissue engineering: Preparation, characterization, and in vitro studies. *J. Biomed. Mater. Res. - Part B Appl. Biomater.* **78**, 47–55.

43 Paraskevopoulos KM, Chatzistavrou X, Goudouri OM, Papadopoulou L, Chrissafis K, Kontonasaki E & Kantiranis N (2009) Study of the Bioactive Behavior of Thermally Treated

Modified 58S Bioactive Glass. *Key Eng. Mater.* **396–398**, 131–134.

44 Summerton J, Hoenig S, Butler C & Chvapil M (1977) The mechanism of hemolysis by silica and its bearing on silicosis. *Exp. Mol. Pathol.* **26**, 113–128.

45 Zhao Y, Sun X, Zhang G, Trewyn BG, Slowing II & Lin VSY (2011) Interaction of mesoporous silica nanoparticles with human red blood cell membranes: Size and surface effects. *ACS Nano* **5**, 1366–1375.

46 Hair ML (1975) Hydroxyl groups on silica surface. *J. Non. Cryst. Solids* **19**, 299–309.

47 Bogdanova A, Makhro A, Wang J, Lipp P & Kaestner L (2013) Calcium in red blood cells-a perilous balance. *Int. J. Mol. Sci.*

48 Nemmar A, Beegam S, Yuvaraju P, Yasin J, Shahin A & Ali BH (2014) Interaction of amorphous silica nanoparticles with erythrocytes in vitro: Role of oxidative stress. *Cell. Physiol. Biochem.* **34**, 255–265.

49 Jiang L, Yu Y, Li Y, Yu Y, Duan J, Zou Y, Li Q & Sun Z (2016) Oxidative Damage and Energy Metabolism Disorder Contribute to the Hemolytic Effect of Amorphous Silica Nanoparticles. *Nanoscale Res. Lett.* **11**, 1–12.

50 Kaestner L, Tabellion W, Lipp P & Bernhardt I (2004) Prostaglandin E2 activates channel-mediated calcium entry in human erythrocytes: An indication for a blood clot formation supporting process. *Thromb. Haemost.* **92**, 1269–1272.

51 Engelmann B (1991) Calcium homeostasis of human erythrocytes and its pathophysiological implications. *Klin. Wochenschr.* **69**, 137–142.

52 Engelmann B & Duhm J (1987) Intracellular calcium content of human erythrocytes: Relation to sodium transport systems. *J. Membr. Biol.* **98**, 79–87.

53 Merciris P, Hardy-Dessources MD & Giraud F (2001) Deoxygenation of sickle cells stimulates Syk tyrosine kinase and inhibits a membrane tyrosine phosphatase. *Blood* **98**, 3121–3127.

54 Ferru E, Giger K, Pantaleo A, Campanella E, Grey J, Ritchie K, Vono R, Turrini F & Low PS (2011) Regulation of membrane-cytoskeletal interactions by tyrosine phosphorylation of erythrocyte band 3. *Blood.*

55 Stefanovic M, Puchulu-Campanella E, Kodippili G & Low PS (2013) Oxygen regulates the band 3–ankyrin bridge in the human erythrocyte membrane. *Biochem. J.* **449**, 143–150.

56 C. C, R. M, A. P, N.E. TF, F. S, E. T, Corbo C, Molinaro R, Parodi A, Toledano Furman NE, Salvatore F & Tasciotti E (2016) The impact of nanoparticle protein corona on cytotoxicity, immunotoxicity and target drug delivery. *Nanomedicine* **11**, 81–100.

Authorship Contributions

I.T and KK designed and executed experiments, interpreted data, were primary contributors to the text and figures and writing of the manuscript

E.K designed experiments, interpreted data, wrote and revised the manuscript

E.L designed experiments, interpreted data and revised the manuscript

G.P designed and executed experiments regarding the characterization of the BGCs

K.R and A.P designed experiments and revised the manuscript

All the co-authors have made significant contributions to improve the manuscript

Conflict of Interest Disclosures. The authors declare no conflict of interest

Figure Legends

Figure 1. *FTIR spectra of produced bioactive glasse ceramics (BGC-T1, BGC-T2, BGC-T3)*

Figure 2. *DLS analysis of synthesized "bioactive glass ceramics"*

Figure 3. a-f : *The variations of Si, Ca, and Mg ions release, measured by ICP method, for two different concentrations (0.25mg/ml, 1mg/ml) and two time points (24 h, 48 h) for all tested BGCs*

Figure 4. *Hemolytic action of BGs in PBS with normal erythrocytes under different conditions of treatment (different temperatures (37 and 40 ^{O}C) and* shaking. *The results are expressed as % of positive control (hemolysis buffer). Data are mean ± SEM (n=6 in each group). * Significant differences to control (-) at $p < .05$ ** $p < .001$*

Figure 5. *Confocal images of erythrocytes after treatment with different concentrations (0.125, 0.5 and 1 mg/ml) of BGC-T2 (scale bar 10 μm)*

Figure 6. *Representative anti-phosphotyrosine immunoblot of Band 3 in erythrocyte membranes from BGC-T2-treated healthy volunteer erythrocytes*

Figure 7. *ROS generation in erythrocytes treated with all the tested BGCs*

Figure 8. *GSH and MDA levels in erythrocytes treated with all the tested BGCs*